Procds. of the 16th Asian Regional Conference on Soil Mechanics and Geotechnical Engineering,
October 14-18, 2019, Taipei, Taiwan

Numerical study on the relationship between inertia and seismic earth thrust acting on an abutment

Keita Abe[1], H. Ikemoto[2], and S. Nomoto[1]

[1] Research and development center, East Japan Railway Company, 2-479, Nisshin-cho, Kita-Ku, Saitama-shi 331-8513, Japan.
[2] Tokyo construction office, Ueno construction zone, East Japan Railway Company, 7-1-1, Ueno, Taito-Ku, Tokyo 110-0005, Japan.

ABSTRACT

Numerical studies were conducted on the seismic behavior of an abutment to investigate the relationship between inertia force and seismic active earth thrust acting on an abutment body. This study determined that lateral active earth thrust could be changed by the magnitude of the inertia force generating an opposite phase between the earth thrust and inertia force. The weight of a girder can influence the magnitude of the seismic active earth thrust.

Keywords: abutment; seismic active earth pressure; inertia

1 INTRODUCTION

Seismic performance evaluations of old-fashioned abutments are important in railway safety to prevent settlement of the backfill due to tilting and sliding of the abutment body. However, it has been observed in a past study (Ikemoto et al., 2016) that the Mononobe–Okabe (M-O) theory (used in a current design code for a railway abutment (RTRI, 2012a and 2012b)) can overestimate the seismic active earth thrust because it is less likely for a large inertia acting on the abutment body and a girder to cause a single-unit movement of the abutment body and backfill that has been assumed in the M-O theory. Hence, we performed numerical simulations of a series of model experiments on the seismic behavior of an abutment to investigate the relationship between inertia force and seismic active earth thrust. In addition, the seismic active earth thrust development corresponding to inertia force acting on an abutment body was investigated by numerical analyses. In this paper, we present our results from the model experiments and numerical analyses, and discuss the relationship between the seismic active earth thrust and inertia force based on our findings.

2 OUTLINE OF MODEL EXPERIMENT

2.1 Experimental model

The schematic figure of the experimental model and the position of the measurement devices are shown in Fig. 1. The abutment model is a 1/8-scale model of a 8.0 m high old fashioned abutment based on the law of similitude proposed by Kagawa (1978). The backfill was placed in a soil tank and was composed of dry No.6 siliceous sand with a 60% relative density. Physical properties of the model soils are listed in Table.1. Colored sands and gauge marks were positioned along a glass side of the soil tank to observe

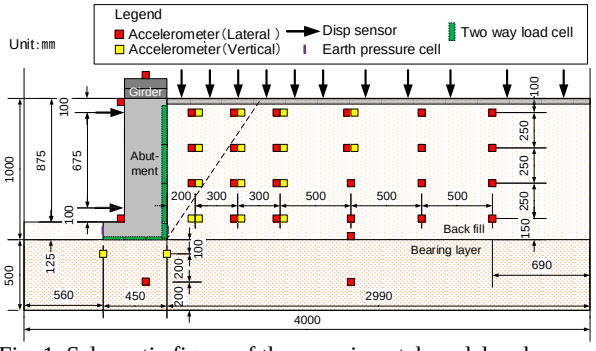

Fig. 1. Schematic figure of the experimental model and position of the measurement devices.

Table. 1. Physical properties of materials used.

Layer	Material	Relative density D_r (%)	Unit weight γ(kN/m^3)	Internal friction angle (c=0.0 kN/m^2)	
				φ_{peak} (°)	φ_{res} (°)
Bearing layer	Tohoku silica sand	80	15.9	42.1	38.6
Backfill	#6	60	15.3	40.3	37.8
Surcharge	Steel grid	–	31.4	–	–

deformation of the backfill. A 1.20 kN/m^2 surcharge (10.0 kN/m^2 in real scale) was loaded onto the backfill surface using steel grids.

The abutment model consists of a 1,488 kg weight steel abutment body. It was constructed so that the unit weight of the model approximated a concrete body. Sandpaper (#80) was installed on the contact surface between the abutment model and soil to simulate frictional force between a concrete body and soil of a real abutment. Two types of abutment bodies were considered; one with a weighted girder (heavy girder type, nearly 28.8 Hz in natural frequency) and the other with a non-weighted girder (light girder type, nearly 43.2 Hz in natural frequency). The center of gravity of

the light girder type was constructed so that the center closely approximated a real abutment with a light steel girder. A 626 kg steel weight was installed on the top of the abutment body in the heavy girder type.

A series of lateral shaking table tests were performed. The input waves were 3.0 Hz sine waves with a wavenumber of 10 and the seismic wave on diluvium requirement for design of railway structures in Japan (137 gal L1 and 944 gal L2 spectrum II (SPII); RTRI, 2012a). The waves were compressed in the direction of the time axes following the law of similitude. The maximum acceleration amplitude of the sine waves was increased stepwise.

2.2 Experimental result

No displacement was seen after shaking both abutment types using the sine waves acceleration below 200 gal and the L1 waves. Backfill settlement in the vicinity of the abutment body was seen in the light girder type after shaking using the 944 gal L2 SPII wave. In comparison, a slippage surface with an angle of rupture of 56° was seen in the backfill of the heavy girder type after shaking using the 944 gal L2 SPII wave as shown in Fig. 2. Subsequently, shaking the heavy girder type using 300 gal sine waves caused increase of the displacement of the abutment body. Lastly, shaking the heavy girder type using the 500 gal sine wave caused rupture of the abutment body.

Time histories of inertia force and lateral earth thrust acting on the abutment body after shaking the heavy girder type using 400 gal sine waves are shown in Fig. 3. Lateral earth thrust and inertia force in the active direction are defined as positive. The lateral earth thrust and inertia force had opposite phases. The lateral earth thrust was at its minimum when the inertia force was at its maximum. Additionally, the variation width of the lateral earth thrust of the heavy girder type was larger than that of the light girder type. These results imply that the lateral active earth thrust can be reduced when the inertia force in the active direction acted on the abutment body.

3 NUMERICAL METHOD AND MODEL

3.1 Numerical method

The material point method (MPM; Sulsky et al., 1994) was used as the numerical method in this study. This method was used because it is easy to derive the deformation of an abutment body and backfill from an elastic small-deformed condition to a large deformed condition with residual displacement (including dynamic response) compared to a conventional method such as the finite element method (FEM).

Calculation process of the MPM is shown in Fig. 4. The numerical analysis target was modeled as a cluster of particles. Stresses of the particles were then calculated using strain increments introduced from back ground meshes. Internal and external force vectors, as

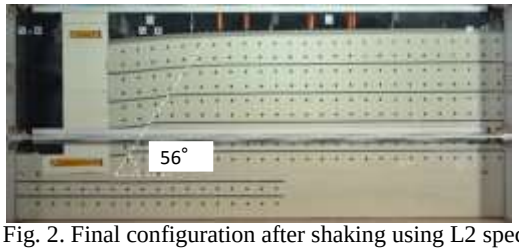

Fig. 2. Final configuration after shaking using L2 spectrum II amplitude of 944 gal obtained from experiment.

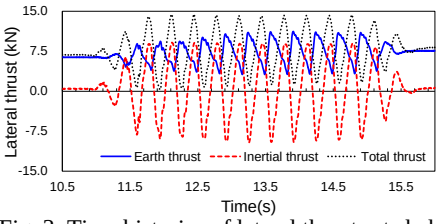

Fig. 3. Time histories of lateral thrusts at shaking heavy girder type using 400gal sine wave obtained from experiment.

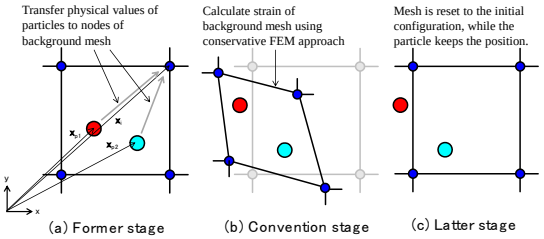

Fig. 4. Calculation process of the MPM.

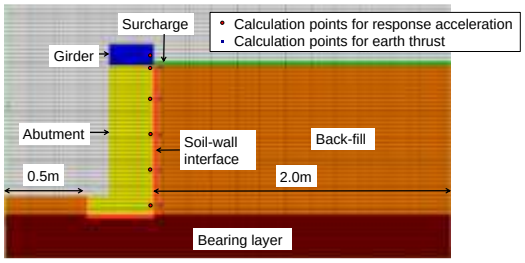

Fig. 5. Numerical analyses model.

Table. 2. Model parameters of the numerical analyses.

Parameters	Values		
	Back fill	Bearing layer	Soil-wall interface
Young's modulus (kPa)	5.0×10^3	5.0×10^3	5.0×10^3
Poisson's ratio	0.30	0.30	0.30
Cohesion (kPa)	1.10	1.40	0.0
Internal friction angle (deg)	39.8	43.8	19.9
Dilatancy angle (deg)	10.0	15.0	0.0
Unit weight (kN/m^3)	15.0	15.6	15.0

well as nodal mass were calculated using stresses, strains, and masses etc. collected at nodal points of the background meshes through interpolation functions (Fig. 4(a)). Velocity vectors were updated using acceleration vectors calculated by the force vectors and nodal masses at the nodal points. Positions of the particles were updated using the velocity vectors. Lastly, stresses of the particles at the next step were calculated from strains of the meshes (Fig. 4(b), (c)).

3.2 Numerical model

Fig. 5 shows the initial state of the numerical model. Length in depth direction was reduced to unit length. Numerical analyses were performed under plain strain condition confining both sides of the 3D numerical model in the depth direction. The particles totaled approximately 5,781 to 5,853 after assigning 1 to 2 particles per 0.025 m × 0.025 m mesh at the initial state. In- and out- plain directions at bottom and left side boundaries were fixed; and the out-plain direction at a right-side boundary was fixed. Surcharge was modeled by assigning one particle with a specific gravity of 4.81 per one mesh. After the initial stresses were obtained with gravity, dynamic analyses were performed using a time explicit scheme for the integration with a 1.0 x 10^{-5} s time interval and 0.002 stiffness dependent damping coefficient referring to Abe et al. (2017).

The stress–strain relationship of the backfill and bearing layer was modeled using an elasto-plasticity model with a Drucker–Prager yield surface and non-associated flow rule. The parameters of the models, which are listed in Table 2, were determined so that simulated values were consistent with experimental values in the tri-axial compression test simulations. The abutment body was modeled as elastic. The frictional forces were modeled by clusters of particles between the abutment body and backfill with elasto-plasticity features of 0.0 kPa in cohesion and half of internal frictional angle of the backfill by referring to a railway abutments design code (RTRI, 2012b). Time histories of acceleration measured by an accelerometer installed in the bearing layer were used as input waves. The inertia forces corresponding to the input waves acted on the particles as external forces.

In this study, experimental results from shaking the heavy and light girder types using 200 gal sine waves and shaking the heavy girder type using 400 gal sine waves, and 944 gal L2 SPII seismic waves were investigated by numerical analyses.

4 NUMERICAL RESULT AND RELATIONSHIP BETWEEN INERTIA AND SEISMIC ACTIVE EARTH THRUST

4.1 Numerical result

Accuracy performance of the numerical method was investigated to reproduce theoretical values of the lateral active earth thrust obtained from the modified M-O theory. Results from the numerical analyses and the modified M-O theory regarding the relationship between the lateral active earth thrust and seismic coefficient are shown in Fig. 6. The lateral active earth thrust was calculated by multiplying horizontal normal stresses of the particles positioned at boundary between back of the abutment body and backfill (see Fig. 5) with sections affected by the stresses. The calculated values were consistent with those obtained from theory when

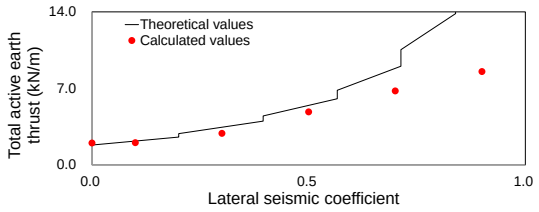

Fig. 6. Lateral earth thrust and seismic coefficient relation obtained from the modified M-O theory and analyses.

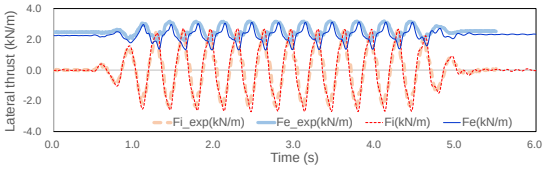

(a) Heavy girder type shaken by 200-gal sine wave.

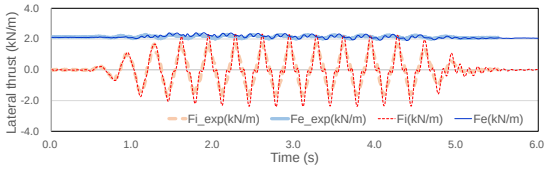

(b) Light girder type shaken 200-gal sine wave.

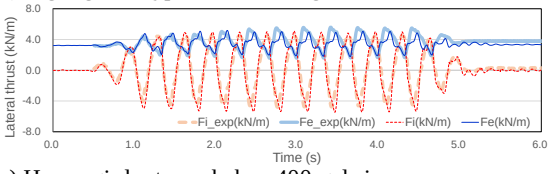

(c) Heavy girder type shaken 400-gal sine wave.

Fig. 7. Time histories of lateral thrusts at shaking using sine waves (experiment: thick line; analyses: thin line).

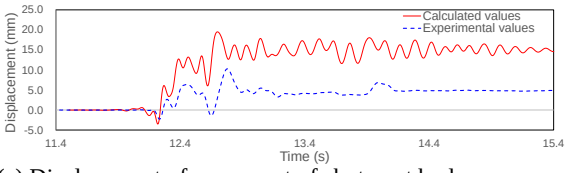

(a) Displacement of upper part of abutment body.

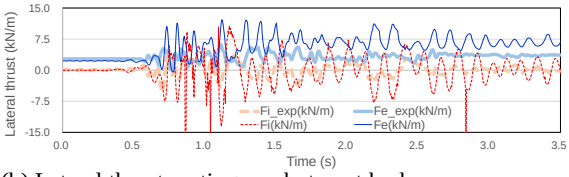

(b) Lateral thrusts acting on abutment body.

Fig. 8. Time histories at shaking heavy girder type using L2 SPII waves (experiment: thick line; analyses: thin line).

the lateral seismic coefficient was small. They were smaller than the theoretical values when the coefficient was large because the active earth thrust decreased depending on the development of displacement of the abutment body, as shown in Watanabe et al. (2011).

Time histories of the lateral earth thrust F_e and inertia force F_i using sine waves obtained from both the numerical analyses and experiments are shown in Fig. 7. The inertia force was calculated by multiplying the horizontal accelerations of the particles positioned in the abutment body (see Fig. 5) with the abutment body masses at shaking. Note that the numerical calculated

values of the lateral earth thrusts at 0.0 s were adjusted to experimental values. The numerical results were consistent with the experimental results, reproducing that the phase of the lateral earth thrust was opposite to that of the inertia force, and the variation width of the lateral earth thrust of the heavy girder type was larger than that of the light girder type. Fig. 8(a) shows time histories of the displacement of an upper part of the abutment body at shaking using the 944 gal L2 SPII waves obtained from the numerical analyses and experiments. Time histories of the F_e and F_i at this shaking case are shown in Fig. 8(b). Inconsistent data of the amplitude, phase and displacement were seen compared to the sine wave shaking cases. This was caused by influence of the numerical noise such as the high frequency of the stresses and accelerations of the particles. The development area of maximum shear strain in the backfill obtained from numerical analyses was largely consistent with that enclosed by the slip surface seen in the experiment and back of the abutment body at this shaking case as shown in Fig. 9. The relationship between numerical calculated values and experimental values, regarding the lateral active earth thrust when the total thrust (= inertia force + lateral earth thrust) was at its maximum value, is shown in Fig. 10. The numerical analyses largely reproduced the experimental result. The calculated values at shaking using the 944 gal L2 SPII seismic wave should be improved upon in future work.

4.2 Relationship between lateral seismic coefficient and lateral active earth thrust

The relationship between the lateral seismic coefficient corresponding to maximum acceleration of the input wave and the lateral active earth thrust when the total thrust was at its maximum value (obtained from the numerical analyses at shaking using the L2 SPII waves and the relationship derived from the modified M-O theory) is shown in Fig. 11. The lateral active earth thrust of the heavy girder case tended to be smaller than that of the light girder case regardless of the magnitude of the lateral seismic coefficient, which was the same trend seen in the model experiment. This indicated that the lateral active earth thrust could be small when the inertia force was large as in the heavy girder case, and the value of the lateral active earth thrust of the heavy girder case could be 1/3 less than that of the light girder case.

5 CONCLUSIONS

Numerical studies of the relationship between the seismic active earth thrust and inertia force acting on the abutment body were conducted. Simulations using the MPM largely reproduced the experimental results regarding seismic behavior of the abutments. It was found that the lateral active earth thrust could be changed by the magnitude of the inertia force

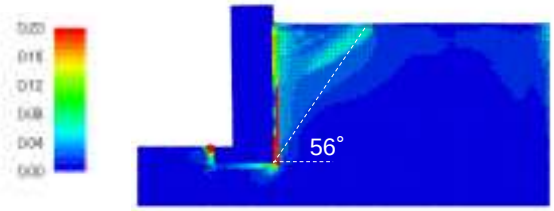

Fig. 9. Distribution of max shear stain in backfill obtained from the numerical analyses at 944 gal L2 SPII shaking.

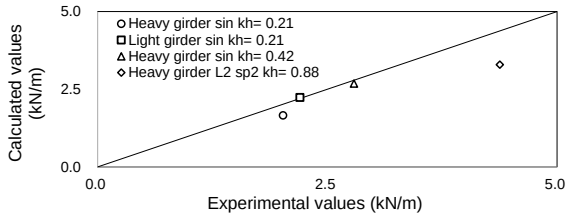

Fig. 10. Numerical calculated values and experimental values relation regarding lateral active earth thrust.

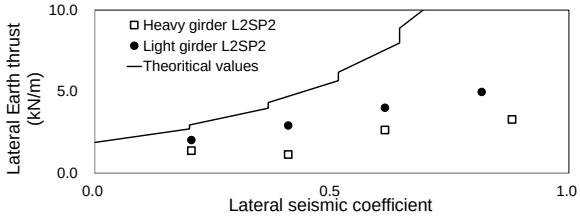

Fig. 11. Lateral active earth thrust and seismic coefficient relation shaken by L2 SPII waves obtained from analyses.

generating an opposite phase between the earth thrust and inertia force. Future studies on the influence of the change in the earth thrust on the stability of the abutment body are required.

REFERENCES

Abe, K., Nakamura, S., Nakamura, H. and Shiomi, K. (2017). Numerical study on dynamic behavior of slope models including weak layers from deformation to failure using material point method, Soils and Foundations, 57, 155-175.

Ikemoto, H., Sanagawa, T., Fujiwara, T., Takasaki, H., and Nishioka, H. (2016). Large-scale shaking table test for confirming seismic behavior of abutment. Proceedings of geotechnical engineering symposium, 201-208 (In Japanese).

Kagawa, T. (1978). On the similitude in model vibration tests of earth-structures, Proceedings of the Japan Society of Civil Engineers, 275, 69-77 (In Japanese).

Railway technical research institute (RTRI). (2012a). Design standards for railway structures and commentary, seismic design (In Japanese).

Railway technical research institute (RTRI). (2012b). Design standards for railway structures and commentary, retaining walls (In Japanese).

Sulsky, D., Chen, Z and Schreyer, H. L. (1994). A particle method for history-dependent materials, Computer Methods in Applied Mechanics and Engineering, 118, 176–196.

Watanabe, K., Koseki, J. and Tateyama, M. (2011). Seismic earth pressure exerted on retaining walls under a large seismic load, Soils and Foundations, 51(3), 379-394.